Available online at www.sciencedirect.com
ScienceDirect
Earth and Planetary Science Letters 265 (2008) 256–269
EPSL
www.elsevier.com/locate/epsl

Perovskite U–Pb ages and the Pb isotopic composition of alkaline volcanism initiating the Permo-Carboniferous Oslo Rift

Fernando Corfu [a,*], Sven Dahlgren [b]

[a] Department of Geosciences, University of Oslo, Postbox 1047 Blindern, N-0316 Oslo, Norway
[b] Regional Centre Buskerud, Telemark and Vestfold, Fylkeshuset, Svend Foynsgate 9, N-3126 Tønsberg, Norway

Received 14 June 2007; received in revised form 13 October 2007; accepted 15 October 2007
Available online 22 October 2007
Editor: R.W. Carlson

Abstract

The Permo-Carboniferous Oslo Rift developed in the foreland of the Variscan orogen over a period of some 50 million years through a process characterized by moderate extension and widespread magmatism. The overall tectonic situation places the Oslo Rift in a post-collisional, dextral transtensional setting related to the convergence between Baltica, Laurentia, Gondwana and Siberia during assembly of Pangea, the location probably reflecting the control by pre-existing lithospheric structures. Although a detailed understanding of these factors and processes relies strongly on having a good age control, the dating of mafic to ultramafic alkalic volcanic units formed during initial rifting has been a very challenging task. In this study we have successfully employed perovskite from melilitic and nephelinitic volcanic rocks, together with magmatic titanite in a more evolved ignimbrite, to obtain ID-TIMS high-precision U–Pb ages. Three samples from various levels of the Brunlanes succession, in the southernmost exposures of the Oslo Graben, yield ages of 300.2±0.9, 300.4±0.7 and 299.9±0.9 Ma. A melililitic tuff at the base of the Skien succession further to the northwest yields a slightly younger age of 298.9±0.7 Ma. The initial Pb compositions derived mainly from coexisting pyroxene, apatite and hornblende are characterized by extremely radiogenic initial $^{206}Pb/^{204}Pb$ ratios (up to 21.3) that confirm a provenance of these early alkaline basalts from HIMU-type sources. The U–Pb ages coincide with the Gzhelian age inferred from fossils in the upper part of the basal rift sedimentary fill of the Asker Group, and post-date the underlying basal sedimentary sequences by some 10 million years, pointing to a relatively rapid initiation of the rifting process.

Keywords: Oslo Rift; alkaline igneous rocks; perovskite; U–Pb ages; HIMU

1. Introduction

Intracontinental rift systems are zones of rupture and deformation of the crust and generally also sites of magmatism. Their development is related to stress imposed on the lithosphere, and to heating or decompression in the underlying mantle. Interpretations of the actual processes and their causes are often controversial and open to debate (e.g. White and McKenzie, 1989; Anderson, 1994). Alkaline basaltic rocks are a common occurrence in continental rifts, especially in the earliest stages of extension, and their genesis is commonly discussed either in terms of partial melting of sublithospheric, enriched mantle domains, or of mantle plumes, or combinations thereof (e.g. Wilson et al., 1995; Späth et al., 2001; Furman et al., 2004; Neumann et al., 2004). It is apparent that the locations of at least some of the continental rifts are controlled by pre-existing lithospheric anisotropies, which can also exert some control on asthenospheric flow patterns and

* Corresponding author. Tel.: +47 22 85 66 80; fax: +47 22 85 42 15.
E-mail address: fernando.corfu@geo.uio.no (F. Corfu).

0012-821X/$ - see front matter © 2007 Elsevier B.V. All rights reserved.
doi:10.1016/j.epsl.2007.10.019

melt generation, as shown for the Baikal Rift (Lebedev et al., 2006).

The Oslo Rift is one well studied example that combines many of the classical features of continental rifts. It developed over a period of some 50 million years, from the end of the Carboniferous throughout much of the Permian, in the foreland of the Variscan Orogen. The rifting was one of the events that accompanied the larger scale assembly of Pangea. It was characterized by a low degree of extension (Pallesen, 1994) and by multistage magmatic activity. The general tectonic setting suggests that rifting was mainly a consequence of regional stretching and thinning of the lithosphere (e.g. Neumann et al., 2004), but the alternative of a mantle plume has also been contemplated (Torsvik et al., 2007). The timing of rifting and magmatism is one of the important parameters for constraining rates of magma emplacement and it is also essential for establishing larger scale correlations. Although quite extensive, the existing geochronological data base for the Oslo Rift has been obtained largely from Rb–Sr whole-rock dating (e.g. Sundvoll and Larsen, 1990, 1993). This system is very susceptible to chemical alteration and Rb–Sr ages of the Oslo Rift can be some 10–30 million years too young because of the protracted hydrothermal activity that accompanied the development of the rift (Dahlgren et al., 1996). Although, U–Pb dating using zircon and baddeleyite provides the means to circumvent this problem, such minerals are absent from the ultramafic to intermediate volcanic rocks that extruded in the initial stages of development of the rift. In this study we have constrained the age of alkaline volcanism using perovskite ($CaTiO_3$), a mineral that has been employed with success in previous geochronological studies of kimberlites and undersaturated basaltic rocks (Heaman, 1989; Kamo et al., 2003; Heaman et al., 2004). We report here U–Pb and Pb–Pb data for perovskite from mafic and ultramafic alkalic rocks located in the Brunlanes and Skien areas, in the southernmost exposures of the Oslo Graben, complemented by U–Pb and Pb–Pb titanite ($CaTiSiO_5$) data for a related ignimbrite, and discuss the implications for the evolution of the Rift.

2. Geological setting

The Oslo Rift comprises two main parts, the Oslo Graben (shown in Fig. 1A) and its extension southward in the North Sea, the Skagerrak Graben. The Oslo Graben is itself subdivided into several en-echelon segments displaced dextrally relative to each other and interpreted to reflect the larger scale dextral Variscan wrench faulting (Olaussen et al., 1994). The rift is located in Proterozoic crust composed mainly of 1600–1500 Ma arc sequences deformed and overprinted by metamorphism and extensively intruded by plutonic rocks between 1400 and 900 Ma (e.g. Bingen et al., 2005). The geometry of the rift appears to have been controlled by pre-exiting structures (Ebbing et al., 2005, 2007), including a distinct topography of the crust-mantle boundary where the craton thickens to the east (Pascal et al., 2004). Modeling shows that melting could have initiated during stretching and thinning of the lithosphere and decompression (Pedersen and van der Beek, 1994; Pascal et al., 2004).

The evolution of the Oslo Rift has been subdivided in six stages: (1) a proto-rift stage, (2) an initial basalt stage, (3) a main plateau-lava and rift-valley stage, (4) a central volcano and cauldron stage, (5) a syenitic batholiths stage, and (6) a termination stage (Sundvoll and Larsen, 1990; Olaussen et al., 1994).

The proto-rift stage was characterized by deposition of mainly fluvial and lacustrine sediments forming the lower parts of the Asker Group (Olaussen et al., 1994). Detrital zircons suggest that the detritus was fed partly from sources in the Variscan orogen to the south (Dahlgren and Corfu, 2001). The initial-rift stage was characterized by emplacement of microsyenitic sills and dykes (called mænaites) in Cambro-Ordovician sedimentary rocks on the flanks of the rift, and by widespread basaltic volcanism (B1), which formed a 800–1500 m thick alkaline basalt sequence in the south changing progressively to a relatively thin (ca. 15 m) tholeiitic sequence farther north (Olaussen et al., 1994; Neumann et al., 2004). The following period was characterized by extensive vertical movements and extensive eruptions of trachyandesitic rhomb porphyry lavas, which were probably related to the intrusion of large larvikite (monzonite) and nepheline syenite complexes. The Larvik plutonic complex has been dated at 298.6±1.4 to 292.1±0.8 Ma (Dahlgren et al., 1996) whereas the Skrim plutonic complex (north of Skien, just off the map in Fig. 1B) is younger at around 281.2±0.6 to 277.3±0.8 Ma (Pedersen et al., 1995). Stage 4 involved the formation of central volcanoes, caldera collapse and graben fill and was followed by the fifth stage characterized by the emplacement of mainly syenitic to granitic batholiths, especially in central and northern parts of the Oslo Rift.

3. The Brunlanes and Skien basalts

The Brunlanes and Skien basaltic series (Fig. 1B) are two of the earliest volcanic assemblages that characterize stage 2 in the formation of the Oslo Rift.

The Brunlanes series consists of olivine–melilititic, melilite–nephelinitic and melilititic lavas in its lower parts, with basanitic flows becoming abundant in the upper part as the sequence evolves progressively into trachybasalt and

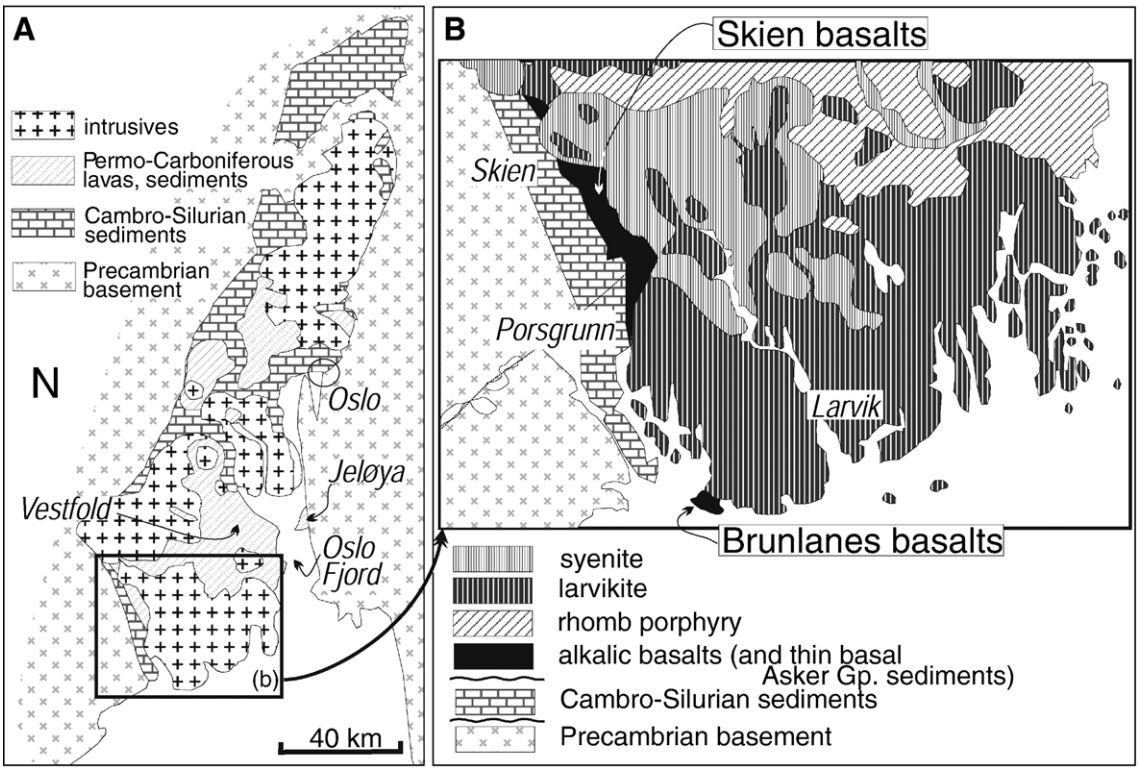

Fig. 1. A) Simplified geological maps of (A) the Oslo Graben, and (B) the study area at the southern end of the Graben.

then ignimbrite. In addition to the flows, there are ca. 8% pyroclastic rocks. The base is not exposed, but it is inferred to be a disconformity or unconformity with the underlying Asker Group sedimentary rocks. The total thickness of the sequence is estimated at about 800 m. These rocks are generally well preserved, retaining detailed volcanic structures and primary mineral compositions. Only the eastern margin of the succession, where it has been intruded by the Larvik plutonic complex, is highly deformed and metamorphosed. Clinopyroxene±olivine+(Cr–Mg) titanomagnetite represent the characteristic phenocrysts of the mafic-ultramafic rocks, but some flows also contain perovskite, melilite (pseudomorphs), phlogopite and apatite phenocrysts. Perovskite occurs as euhedral to subhedral phenocrysts in the matrix but it is also observed as submicroscopic inclusions in pyroxene.

Two samples from the second-lowest set of flows exposed at Brunlanes yielded perovskite. Sample A is a pyroclastic rock representing an ultramafic surge. The overlying melilitite flow provided sample B. The third sample, from a higher stratigraphic level of the Brunlanes succession, is a hornblende-and titanite-bearing ignimbrite (D). The hornblende is locally altered to biotite whereas the titanite occurs as sharp euhedral and unaltered phenocrysts.

The Skien series consists of nephelinites, basanites and alkali basalts. The succession overlies the clastic sedimentary rocks of the Asker Group starting with a thin black quartzite layer, followed by laminated melilitic tuff, massive black melilitic tuff, and massive brown-beige syenitic tuff, the whole ca. 30 m thick. Above that there is a 1250 m thick sequence of nephelinites, which evolve upwards to basanites and alkali basalts (Segalstad, 1979). The laminated melilitic tuff near the base contains perovskite and was collected for dating (sample C). In contrast to the Brunlanes samples, however, the tuff in the Skien succession is altered to carbonate, very fine-grained opaque matter and chlorite and the pyroxene is almost entirely retrogressed. The perovskite occurs as homogeneous and, mostly, perfectly euhedral phenocrysts, with some fractures but essentially no inclusions or internal alteration. Apatite also forms sharp euhedral crystals. Magnetite can include perovskite and is locally altered.

4. U–Pb and Pb–Pb geochronology

4.1. Analytical procedure

The rocks were crushed and separated using, sequentially, jaw crusher, hammer mill, Wilfley table,

magnetic separation and heavy liquids. Perovskite and titanite occur mainly in fractions of intermediate magnetic susceptibility and the fractions to be analyzed were handpicked under a binocular microscope. After washing and weighing the grains were transferred to Savillex vials, spiked and dissolved on a hot-plate in HF (+HNO_3) for several days. Spiking was done initially with a mixed $^{205}Pb/^{235}U$ spike and subsequently with a double $^{205}Pb/^{202}Pb/^{235}U$ spike. The analyses were done over a period of time while developing and testing a simplified chemical separation procedure, which fixes and purifies Pb and U on anion exchange resin with a mixture of 3 N HCl+0.5 N HBr through one single column step (Corfu and Andersen, 2002). Pyroxene, apatite and hornblende were treated in the same manner, but magnetite had to be processed with 1 N HBr to clean the Pb, purifying the U in a separate 7 N HNO_3 step. Some fractions were split to test variations in the procedure. The variable quality of some of the data reflects in part these tests, a fact taken in consideration during the evaluation. Overall the reproducibility demonstrated by the various split fractions is satisfactory as they overlap within the independently estimated analytical uncertainty (Tables 1 and 2). The results were plotted and calculated using Isoplot (Ludwig, 2003) and the decay constants of Jaffey et al. (1971).

4.2. Perovskite in samples A, B, C

Perovskite is identified in the mineral separates of samples #A, B and C and occurs as fragments, generally black and opaque and less commonly translucent to nearly transparent with brown, lilac or olive colours.

The U content is highest in perovskite from B at 58–75 ppm, and somewhat lower in those from A (38–46 ppm) and C (29–44 ppm) (Table 1). The Th/U ratios tend to be high at 7–12 in A, 3–5 in B and 3–7 in C. The content of initial Pb also varies from sample to sample with the highest levels of 2–4 ppm in A, 2–1.5 ppm (but with one value of 10 ppm) in B and 1.4–0.7 ppm in C. Although undetected inclusions of other minerals may be responsible for some of the higher common Pb values, thin section examination shows that the perovskite is mostly clean and free of inclusions and hence the general initial Pb level is likely to be a property of the mineral. This initial common Pb component accounts for about 20 to 40% of the total Pb present in the sample, with $^{206}Pb/^{204}Pb$ ratios mostly around 110–160 in sample B, 125–115 in C and 50–90 in A, hence the initial Pb composition plays an important role in defining the age.

The composition of the initial Pb can be estimated, to some degree, from the perovskite data alone, exploiting variations in the ratio between radiogenic and common Pb. In general, however, the extrapolations tend to be quite large and the inferred ratios imprecise. Moreover, in sample C the spread is very limited. To obtain more accurate estimates of the common Pb compositions, coexisting pyroxene in A and B, and apatite in C were analyzed. Magnetite was also measured in A, but its composition does not match that of pyroxene, probably due to retrogression, as discussed below.

When plotted in isochron diagrams (Figs. 2 and 3) the data for all three samples define statistically valid regressions yielding ages that overlap mostly within error. The $^{238}U/^{206}Pb$ ages, however, are systematically older than the corresponding $^{235}U/^{207}Pb$ ages.

An alternative way to view the data is by plotting them, uncorrected for initial Pb, in the 3-dimensional concordia plot (Ludwig, 2003). In this plot the fit of the data is less good than in the isochron diagrams, most likely because only one of the plotted ratios ($^{238}U/^{206}Pb$, $^{207}Pb/^{206}Pb$, $^{204}Pb/^{206}Pb$) is affected by the higher uncertainty associated with the measurement of ^{204}Pb. The linear 3D regressions for samples B and C can accommodate all the data with MSWD values of 1.9 and 1.6, respectively.

By contrast it is not possible to fit all the data points of sample A on one single line. There is a most obvious divergence between the $^{238}U/^{206}Pb$ ratio of pyroxene and that of magnetite, indicating that the two minerals were not in isotopic equilibrium. Calculation of ten data points for perovskite alone yields an MSWD of 1.7 but a significantly higher age (305.1±2.0) than by including magnetite in the regression (302.7±0.6 Ma with MSWD=2.2). The MSWD increases to 3.8 for a regression through perovskite and pyroxene data points, in this case lowering the age to 300.7±1.1. Exclusion of one perovskite data point (Table 2) from the line through perovskite and pyroxene reduces the MSWD to 2.5 defining an age of 300.2±0.9 Ma, which is our preferred age (Fig. 2). This choice is supported by three arguments. First, pyroxene is a magmatic phase and hence its composition is most likely to approach that of the magmatic system whereas magnetite exhibits local evidence of subsolidus transformations suggesting that it was affected by later processes. Second, this case is very similar to that of the ignimbrite (D) data discussed below, where the U–Pb composition of magnetite shows the effects of later Pb loss and the ratio plots distinctly above the 3D-linear isochron. Third, the age matches that of sample B collected from a slightly higher level of the same lithostratigraphic unit, the petrologic affinity and lack of significant weathering and erosion arguing against the existence of a large time gap between the extrusion of these flows.

Table 1
Concentrations and isotopic data corrected for initial common Pb

Fraction	Weight	Pb]	U	Th/U	Pbc	$^{207}Pb/^{235}U$	2 sigma	$^{206}Pb/^{238}U$	2 sigma
	[mg]	[ppm]	[ppm]		[ppm]		[abs]		[abs]
(a)	(b)	(b)	(b)	(c)	(d)	(e)	(e)	(e)	(e)
Sample A: volcanoclastic ultramafic rock, Saltstein, Brunlanes, M2V2 (C-01-120; 58°58′6.0/9°50′19.5)									
P bl op*	0.087	7.4	38.8	7.1	1.94	0.3507	0.0112	0.04824	0.00020
P b op	0.105	10.1	44.3	12.1	1.98	0.3416	0.0077	0.04814	0.00029
P bl trl	0.770	10.8	43.9	12.0	2.23	0.3452	0.0084	0.04808	0.00032
P b op	0.240	11.6	42.4	11.4	4.31	0.3514	0.0148	0.04779	0.00025
Aliquot		11.6	42.4	10.2	4.31	0.3502	0.0166	0.04767	0.00027
P lil-b trl	0.592	12.4	46.5	10.6	4.13	0.3504	0.0128	0.04784	0.00021
Aliquot		12.3	46.4	9.9	4.13	0.3306	0.0117	0.04758	0.00020
P lil-b trl	0.382	11.0	37.6	10.6	4.14	0.3464	0.0128	0.04763	0.00015
Aliquot		11.0	37.6	10.7	4.12	0.3465	0.0108	0.04762	0.00012
P b trl	0.074	9.5	40.4	10.4	2.74	0.3399	0.0104	0.04768	0.00019
PX y-b	9.655	0.13	0.048	8.3	0.118	–	–	–	–
MT fr-eu	6.361	7.4	3.1	5.9	6.76	–	–	–	–
Aliquot		7.5	3.1	5.8	6.86	–	–	–	–
Sample B: olivine melilitite flow, Saltstein, Brunlanes, M2F2 (C-01-121; 58°58′6.0/9°50′19.5)									
P lil-ol op	0.140	15.8	57.6	4.6	10.16	0.3498	0.0174	0.04772	0.00025
P lil-ol op	0.199	7.8	63.6	4.0	1.67	0.3402	0.0033	0.04760	0.00010
Aliquot		7.8	63.6	4.0	1.64	0.3429	0.0037	0.04770	0.00013
P bl-op	0.517	8.5	64.1	4.2	2.09	0.3502	0.0077	0.04781	0.00036
P bl-op	0.082	8.5	68.3	4.2	1.85	0.3427	0.0058	0.04767	0.00021
P bl-op	0.130	8.4	74.8	3.4	1.80	0.3415	0.0039	0.04753	0.00016
P b trl*	0.057	8.3	71.2	4.2	1.63	0.3410	0.0045	0.04792	0.00026
P bl-op*	0.105	8.9	74.4	4.6	1.93	0.3371	0.0049	0.04780	0.00019
PX y-b	6.135	0.055	0.033	4.8	0.050	–	–	–	–
Sample C: laminated melilititic tuff, below Skien basalts, Kjerringsåsen, Porsgrunn (C-05-1 (KJÅ-23); 59°8′43.7/9°41′57.7)									
P b-ol tr-trl*	0.082	4.9	41.3	3.2	1.35	0.3391	0.0062	0.04743	0.00014
P b-r trl*	0.249	4.7	28.7	6.9	0.89	0.3449	0.0047	0.04760	0.00014
P b-r op	0.474	6.4	44.1	5.3	1.36	0.3399	0.0059	0.04746	0.00014
Aliquot		6.3	44.1	5.5	1.35	0.3430	0.0058	0.04734	0.00015
P b-r op	0.060	3.2	23.4	5.0	0.70	0.3419	0.0062	0.04719	0.00029
AP	0.209	0.075	0.018	5.3	0.07	–	–	–	–
Sample D: ignimbrite, Skarvholmen, Brunlanes (C-01-4, 16.2000 E; 58°56′55.4/9°53′42.7)									
T fr-eu b abr	0.087	3.1	16.4	6.1	1.05	0.355	0.013	0.04821	0.00023
T fr-eu b abr	0.179	2.9	13.9	17.7	1.10	0.318	0.037	0.04787	0.00044
T fr-eu b	0.103	2.7	14.2	6.6	0.85	0.3412	0.0091	0.04758	0.00013
T fr-eu b	0.363	2.9	15.0	7.3	0.95	0.337	0.045	0.04748	0.00086
T fr-eu b	0.276	2.7	14.8	9.0	0.77	0.329	0.016	0.04736	0.00082
T fr-eu b	0.222	2.8	16.2	6.4	0.75	0.3343	0.0081	0.04723	0.00019
T fr-eu b	0.161	2.6	14.9	6.6	0.71	0.3466	0.0099	0.04773	0.00019
Aliquot		2.6	14.9	6.3	0.71	0.3393	0.0073	0.04755	0.00013
MT	0.675	2.0	6.7	2.2	1.54	0.302	0.025	0.04406	0.00019
HBL	0.528	9.1	6.2	5.1	8.13	–	–	–	–

a) P=perovskite, T=titanite; PX=pyroxene; MT=magnetite; AP=apatite; HBL=hornblende; eu=euhedral; fr=fragment; b=brown; lil=lillac; r=red; bl=black; y=yellow; ol=olive; tr=transparent; trl=translucent; op=opaque; abr=abraded before analysis; *=not used in age calculation.
b, d) Weight and concentrations are known to better than 10%.
c) Th/U model ratio inferred from 208/206 ratio and age of sample.
d) Pbc=initial common Pb (corrected for blank).
e) Corrected for fractionation, spike, blank and initial common Pb (values from linear 3D-isochron, Figs. 2 and 3); error calculated by propagating the main sources of uncertainty.

Correlation coefficient	$^{207}Pb/^{206}Pb$	2 sigma [abs]	$^{206}Pb/^{238}U$	2 sigma [abs]	$^{207}Pb/^{235}U$	2 sigma [abs]	$^{207}Pb/^{206}Pb$	2 sigma [abs]
(e)	(e)	(e)	(e)	(e)	(e)	(e)	(e)	(e)
0.57	0.0527	0.0016	303.7	1.2	305.3	8.4	317	67
0.38	0.0515	0.0011	303.1	1.8	298.4	5.7	262	47
0.47	0.0521	0.0011	302.7	2.0	301.1	6.1	289	50
0.49	0.0533	0.0021	300.9	1.5	305.7	11.1	343	88
0.54	0.0533	0.0024	300.2	1.6	304.9	12.4	341	98
0.49	0.0531	0.0018	301.2	1.3	305.0	9.6	334	77
0.45	0.0504	0.0017	299.6	1.2	290.0	8.9	213	76
0.57	0.0527	0.0019	300.0	0.9	302.0	9.6	318	79
0.46	0.0528	0.0016	299.9	0.7	302.1	8.1	319	67
0.48	0.0517	0.0015	300.2	1.2	297.1	7.7	272	65
–	–	–	–	–	–	–	–	–
–	–	–	–	–	–	–	–	–
–	–	–	–	–	–	–	–	–
0.27	0.0532	0.0026	300.5	1.6	304.6	13.0	336	110
0.47	0.0518	0.0005	299.8	0.6	297.3	2.5	278	20
0.48	0.0521	0.0005	300.4	0.8	299.4	2.8	292	22
0.50	0.0531	0.0010	301.1	2.2	304.9	5.8	334	43
0.42	0.0521	0.0008	300.2	1.3	299.2	4.4	291	35
0.50	0.0521	0.0005	299.3	1.0	298.3	2.9	290	23
0.52	0.0516	0.0006	301.8	1.6	297.9	3.4	268	26
0.44	0.0512	0.0007	301.0	1.1	295.0	3.7	248	30
–	–	–	–	–	–	–	–	–
0.30	0.0519	0.0009	298.8	0.8	296.5	4.7	279	40
0.39	0.0525	0.0007	299.8	0.8	300.9	3.6	309	29
0.32	0.0520	0.0009	298.9	0.9	297.1	4.5	283	38
0.31	0.0526	0.0009	298.2	0.9	299.5	4.4	310	36
0.29	0.0525	0.0009	297.2	1.8	298.6	4.6	309	39
–	–	–	–	–	–	–	–	–
0.49	0.0534	0.0018	303.5	1.4	308.3	9.5	344	74
0.84	0.0482	0.0053	301.4	2.7	280.2	28.2	–	–
0.56	0.0520	0.0013	299.6	0.8	298.1	6.9	286	57
0.57	0.0515	0.0064	299.0	5.3	295.0	33.5	263	262
0.46	0.0503	0.0021	298.3	5.0	288.5	11.8	210	95
0.48	0.0513	0.0012	297.5	1.2	292.9	6.1	256	51
0.52	0.0527	0.0014	300.6	1.1	302.1	7.4	314	60
0.47	0.0518	0.0010	299.4	0.8	296.6	5.5	275	46
0.45	0.0498	0.0041	278.0	1.193	268.2	19.6	183	184
–	–	–	–	–	–	–	–	–

Table 2
Isotopic data, not corrected for initial common Pb

Fraction	$^{238}U/^{204}Pb$	2s%	$^{206}Pb/^{204}Pb$	2s%	$^{235}U/^{204}Pb$	2s%	$^{207}Pb/^{204}Pb$	2s%	$^{238}U/^{206}Pb$	2s%	$^{207}Pb/^{206}Pb$	2s%	$^{204}Pb/^{206}Pb$	2s%
(a)	(b)	(b)	(b)	(b)	(b)	(b)	(b)	(b)	(b)	(b)	(b)	(b)	(b)	(b)
Sample A: volcanoclastic ultramafic rock, Saltstein, Brunlanes, M2V2 (C-01-120; 58°58′6.0/9°50′19.5)														
P bl op*	1307.27	0.91	83.63	0.80	9.481	0.91	19.01	0.65	15.63	0.37	0.22731	0.15	0.01196	0.80
P b op	1462.33	0.72	90.97	0.63	10.606	0.72	19.31	0.44	16.08	0.59	0.21226	0.33	0.01099	0.63
P bl trl	1283.26	0.73	82.26	0.43	9.307	0.73	18.90	0.40	15.60	0.66	0.22971	0.17	0.01216	0.43
P b op	638.49	0.38	51.08	0.29	4.631	0.38	17.31	0.36	12.50	0.41	0.33891	0.11	0.01958	0.29
Aliquot	640.00	0.46	51.09	0.37	4.643	0.46	17.31	0.43	12.53	0.45	0.33882	0.10	0.01957	0.37
P lil-b trl	736.10	0.40	55.79	0.33	5.339	0.40	17.56	0.37	13.20	0.34	0.31471	0.10	0.01793	0.33
Aliquot	734.01	0.31	55.49	0.27	5.324	0.31	17.45	0.32	13.23	0.30	0.31436	0.10	0.01802	0.27
P lil-b trl	592.61	0.29	48.80	0.22	4.298	0.29	17.17	0.26	12.14	0.31	0.35195	0.10	0.02049	0.22
Aliquot	597.19	0.21	49.01	0.13	4.331	0.21	17.19	0.19	12.19	0.26	0.35068	0.10	0.02040	0.13
P b trl	962.10	0.68	66.44	0.54	6.978	0.68	18.06	0.41	14.48	0.33	0.27177	0.12	0.01505	0.54
PX y-b	25.31	2.98	21.77	0.86	0.184	2.98	15.71	0.86	1.163	3.10	0.72160	0.12	0.04593	0.86
MT fr-eu	29.33	0.38	21.78	0.15	0.213	0.38	15.77	0.20	1.347	0.41	0.72408	0.10	0.04592	0.15
Aliquot	28.70	0.42	21.73	0.23	0.208	0.42	15.77	0.26	1.321	0.47	0.72572	0.10	0.04603	0.23
Sample B: olivine melilitite flow, Saltstein, Brunlanes, M2F2 (C-01-121; 58°58′6.0/9°50′19.5)														
P lil-ol op	375.46	0.21	39.23	0.13	2.72	0.21	16.72	0.19	9.57	0.53	0.42607	0.10	0.02549	0.13
P lil-ol op	2527.30	0.42	141.61	0.36	18.33	0.42	22.00	0.28	17.85	0.22	0.15533	0.10	0.00706	0.36
Aliquot	2568.74	0.48	143.83	0.41	18.63	0.48	22.15	0.34	17.86	0.27	0.15401	0.11	0.00695	0.41
P bl-op	2029.11	1.07	118.33	0.75	14.72	1.07	20.92	0.65	17.15	0.75	0.17675	0.13	0.00845	0.75
P bl-op	2450.79	0.97	138.15	0.62	17.78	0.97	21.85	0.62	17.74	0.45	0.15818	0.22	0.00724	0.62
P bl-op	2734.70	0.63	151.45	0.52	19.83	0.63	22.57	0.39	18.06	0.34	0.14899	0.10	0.00660	0.52
P b trl	2894.33	1.30	160.02	1.11	20.99	1.30	22.92	0.58	18.09	0.54	0.14323	0.28	0.00625	1.11
P bl-op	2555.68	0.78	143.46	0.67	18.54	0.78	22.01	0.51	17.81	0.39	0.15342	0.16	0.00697	0.67
PX y-b	41.41	3.53	23.28	0.82	0.30	3.54	15.90	0.37	1.779	3.62	0.68288	0.68	0.04296	0.82
Sample C: laminated melilititic tuff, below Skien basalts, Kjerringsåsen, Porsgrunn (C-05-1 (KJÅ-23); 59°8′43.7/9°41′57.7)														
P b-ol tr-trl	1998.63	1.02	115.15	0.87	14.50	1.02	20.57	0.42	17.36	0.29	0.17865	0.10	0.00868	0.87
P b-r trl	2107.74	0.60	120.68	0.52	15.29	0.60	20.93	0.38	17.47	0.28	0.17341	0.10	0.00829	0.52
P b-r op	2118.15	0.41	120.86	0.36	15.36	0.41	20.88	0.36	17.53	0.30	0.17273	0.10	0.00827	0.36
Aliquot	2129.85	0.40	121.16	0.34	15.45	0.40	20.95	0.35	17.58	0.31	0.17294	0.10	0.00825	0.34
P b-r op	2184.20	2.62	123.41	2.24	15.84	2.62	21.07	0.78	17.70	0.61	0.17075	0.34	0.00810	2.24
AP	16.27	7.52	21.13	1.07	0.118	7.52	15.72	0.49	0.770	7.59	0.74389	0.34	0.04733	1.07
Sample D: ignimbrite, Skarvholmen, Brunlanes (C-01-4, 16.2000 E; 58°56′55.4/9°53′42.7)														
T fr-eu b abr	1002.20	6.02	67.73	4.40	7.27	6.02	18.26	1.03	14.80	0.47	0.26959	0.19	0.01476	4.40
T fr-eu b abr	812.37	3.07	58.30	2.31	5.89	3.07	17.55	1.42	13.93	0.91	0.30110	0.16	0.01715	2.31
T fr-eu b	1068.52	1.25	70.25	0.94	7.75	1.25	18.32	0.41	15.21	0.26	0.26085	0.11	0.01424	0.94
T fr-eu b	1012.77	2.47	67.49	2.25	7.35	2.47	18.16	2.12	15.01	1.81	0.26901	0.73	0.01482	2.25
T fr-eu b	1238.07	1.84	78.04	0.95	8.98	1.84	18.63	0.79	15.86	1.72	0.23874	0.46	0.01281	0.95
T fr-eu b	1384.93	0.78	84.83	0.62	10.04	0.78	19.038	0.44	16.33	0.41	0.22444	0.15	0.01179	0.62
T fr-eu b	1348.06	1.13	83.76	0.93	9.78	1.13	19.07	0.58	16.09	0.57	0.22766	0.28	0.01194	0.93
Aliquot	1352.20	0.99	83.70	0.79	9.81	0.99	19.01	0.40	16.15	0.28	0.22708	0.13	0.01195	0.79
MT	278.02	0.25	31.660	0.15	2.016	0.25	16.289	0.21	8.781	0.44	0.51450	0.15	0.03159	0.15
HBL	48.064	0.23	21.690	0.13	0.349	0.23	15.799	0.20	2.216	0.40	0.72840	0.13	0.04610	0.13

a) P=perovskite, T=titanite; PX=pyroxene; MT=magnetite; AP=apatite; HBL=hornblende; eu=euhedral; fr=fragment; b=brown; lil=lillac; r=red; bl=black; y=yellow; ol=olive; tr=transparent; trl=translucent; op=opaque; abr=abraded before analysis; *=not used in 3-D regression.
b) Corrected for fractionation, spike and blank; error calculated by propagating the main sources of uncertainty.

In the normal Wetherill diagrams, at the bottom of Figs. 2 and 3, the U–Pb ratios are plotted after correcting for common Pb using the compositions determined in the 3D-isochron calculation. This is essentially an image of the projection of the data from 3D space onto the radiogenic isotope plane. Although strictly speaking redundant, the plot brings out some details of the data not quite evident in the other representations, possibly because of not quite identical ways of calculating the analytical uncertainties. The plot for sample A highlights the

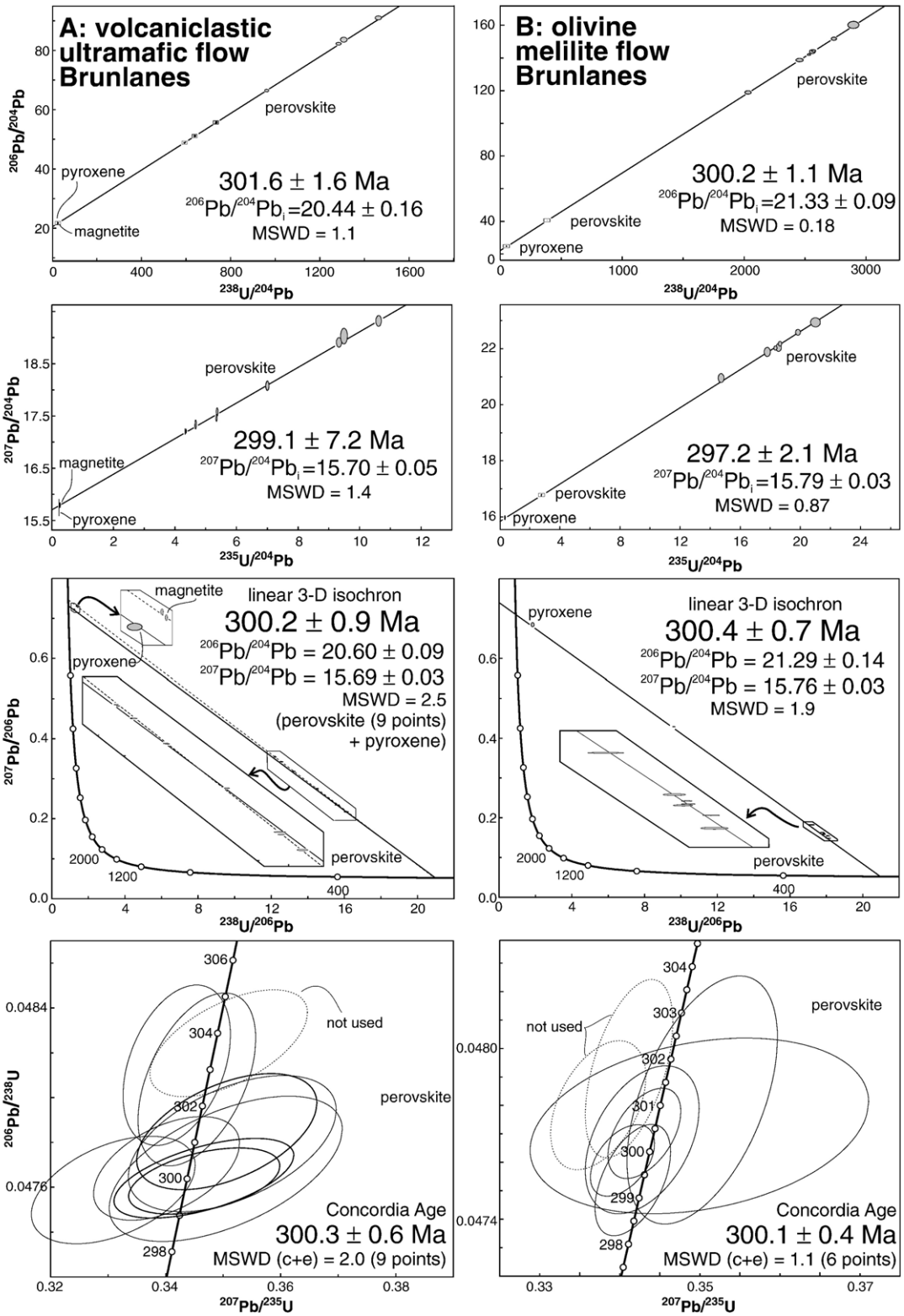

Fig. 2. Isochron diagrams (top), a 3-D concordia diagram, and a 2-D Wetherill-type concordia diagrams (bottom) for Pb–Pb and U–Pb data for the two mafic-ultramafic volcanic rocks of the Brunlanes section. Uncertainties represent 2 sigma. Data are given in Tables 1 and 2.

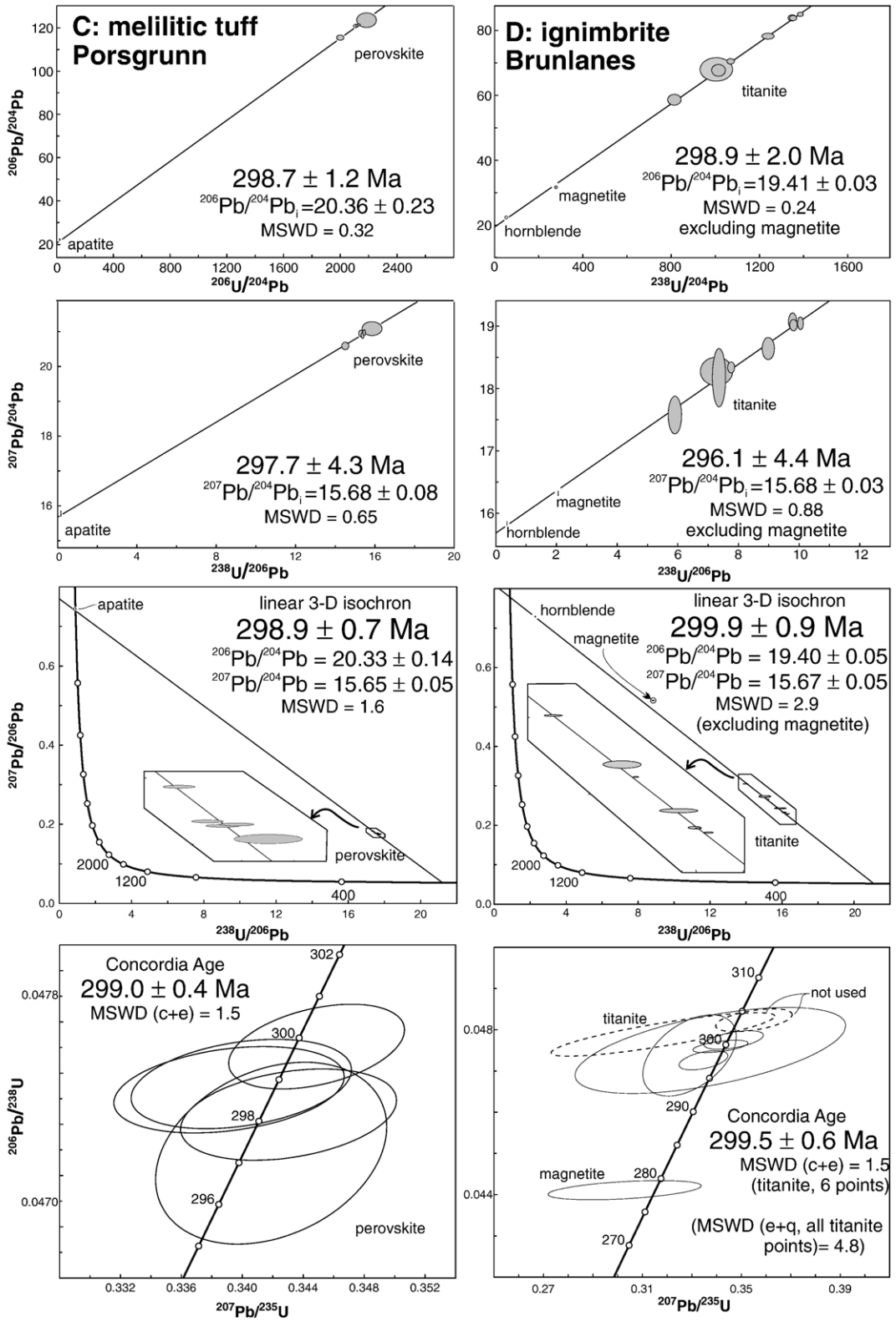

Fig. 3. Isochron diagrams (top), a 3-D concordia diagram, and a 2-D Wetherill-type concordia diagram (bottom) for Pb–Pb and U–Pb data for a tuff at the base of the Skien alkali basalt sequence (C) and an ignimbrite high in the Brunlanes sequence (D). Uncertainties represent 2 sigma. Data are given in Tables 1 and 2.

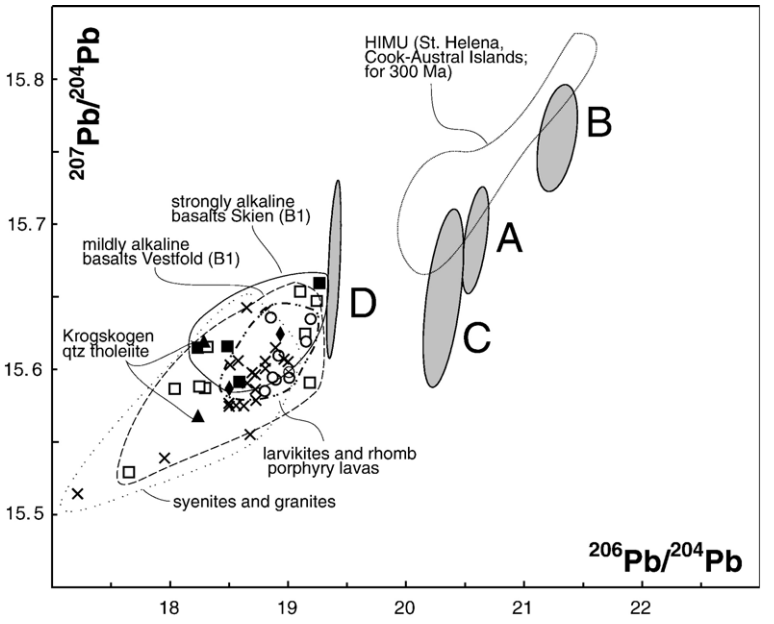

Fig. 4. Initial Pb isotopic ratios of the four samples from Brunlanes and Porsgrunn (A–D; ellipses indicating the analytical uncertainty). Also shown is the distribution of whole rock Pb isotopic data for other units of the Oslo rift: ■=strongly alkaline B1 basalts, Skien; □=mildly alkaline B1 basalts, Vestfold; ▲=B1 quartz tholeiite, Krogskogen; ◆=rhomb porphyry lavas, Krogskogen; ○=larvikites; ×=syenites and granites. Data are from Neumann et al. (1988) and Trønnes and Brandon (1992), and are corrected for an age of 300 Ma. The field for HIMU rocks is based on data from Stracke et al. (2005) calculated backwards for an age of 300 Ma using a μ-value = 10.

position of the one outlier already excluded from the 3D regression, that also destroys the equivalence of the data set. A concordia age calculated through the other nine data points has an MSWD (of concordance and equivalence) of 2.0 and an age of 300.3±0.6 Ma, basically the same as in the 3D-isochron. The plot for sample B also reveals two outliers with too low $^{207}Pb/^{235}U$ ratios (Table 1). The remaining six data points yield a concordia age of 300.1±0.4 Ma. In both cases the reasons for the outliers are probably related to the measurement rather than to natural causes. All five data points of sample C show a good fit and yield a concordia age of 299.0±0.4 Ma.

4.3. Titanite in ignimbrite (C)

Titanite occurs as euhedral sphenoidal crystals, in the mineral separates generally as broken fragments, brown and transparent, but commonly with small inclusions of other minerals. The titanite contains 14–16 ppm U and has high Th/U of 6–9 with one at 18 (Table 2). Its initial common Pb content of 1.0–0.7 ppm is relatively low for titanite, but sufficiently high to introduce large uncertainties in the calculation of the radiogenic Pb composition. Hornblende and magnetite were analyzed to determine the initial Pb composition.

The titanite data points are collinear when plotted in the $^{206}Pb/^{204}Pb$ versus $^{238}U/^{204}Pb$ isochron diagram (Fig. 3) and they fit on lines through either hornblende or magnetite, but not through both. The different regressions yield ages varying by 6 m.y. The deviation is less pronounced, but still evident, in the $^{207}Pb/^{204}Pb$ versus $^{235}U/^{204}Pb$ isochron diagram.

The two concordia plots reveal a number of complications in the data pattern. The best resolution is given by the Wetherill diagram which highlights the much younger apparent age of magnetite with respect to titanite, suggesting Pb loss or some other subsolidus process such as alteration that affected the U–Pb ratios. The titanite data plot within error on the concordia curve but with a distinct dispersion in $^{206}Pb/^{238}U$ and it is necessary to omit the two top points (Table 1) to achieve an acceptable probability of fit and calculate a concordia age. The deviation of the magnetite data point from the array of the other analyses is also very obvious in the 3D-plot. Omitting the two analyses with low $^{238}U/^{206}Pb$ (Table 2) reduces the MSWD to 1.2 and the age to 299.4±0.5 Ma. These two analyses were carried out in a test phase before the bulk of the project and it is possible that they may be somewhat biased. It is thus not quite evident whether the scatter is due to analytical factors (such as incomplete dissolution or the measurement) or to geological factors.

The age of 299.9±0.9 Ma obtained from the 3D-linear isochron of titanite and hornblende is preferred at this stage.

4.4. Initial Pb compositions

The initial Pb compositions for the four samples are characterized by very radiogenic $^{206}Pb/^{204}Pb$ ratios ranging from 21.29 for sample B to 19.40 for sample D (Figs. 2 and 3). They are positively correlated to $^{207}Pb/^{204}Pb$ ratios of 15.76 to 15.67 (Fig. 4).

5. Discussion

5.1. Rift chronology

The Brunlanes alkalic basalts are among the earliest magmatic products of the Oslo Rift. The ages obtained for this sequence at 300.4±0.7 to 299.9±0.9 Ma are, thus, a good estimate for initiation of magmatic activity during rifting (Fig. 5). The melilitic tuff at the base of the Skien succession yields a slightly younger age of 298.9±0.7 Ma suggesting that the northward decrease in alkalinity may also reflect a temporal trend. If technically feasible, dating of the B1 tholeiitic basalts further north in the Oslo Rift could be used to verify this apparent trend of decreasing alkalinity with time and latitude.

Another magmatic expression of these initial episodes of rifting was the intrusion of microsyenitic ("mænaite") sills and dykes in the Cambro-Ordovician cover on the flanks of the rift (Sundvoll et al., 1992). One of these has been dated at 300±1 Ma by zircon U–Pb in the Langesund area (Corfu and Dahlgren, unpubl. data).

The basalts at Brunlanes and Skien overlay fluvial sedimentary deposits of the Asker Group. This Group comprises two main parts. The lower and middle deltaic successions have been assigned to the proto-rift stage (Olaussen et al., 1994). They contain evidence for a local marine incursion, with foraminifera indicative of a Moscovian age, about 310 Ma according to the Time Scale of Gradstein et al. (2004). The upper deltaic succession and overlying volcanoclastic alluvial fans are correlated instead with the initial-rift stage. Fossils of fresh water mussels found near the bottom of this deltaic sequence have been assigned to the terminal Gzhelian stage of the Carboniferous (Eagar, 1994), i.e. the period between 303.9 and 299.0 Ma (Gradstein et al., 2004). Thus, the late stages of deposition of the Asker Group and extrusion of the overlying basalts were crudely coincident, as demonstrated by the overlapping ages (this study) and also by the presence of clasts of alkali basalt in the alluvial fans (Olaussen et al., 1994).

Formation of the early basalt sequences was followed by intrusion of the Larvik plutonic complex, a set of nested, circular bodies emplaced progressively from east to west and then to the northwest from 298 to 290 Ma (Petersen 1978; Dahlgren et al., 1996). This period probably also encompassed the eruption of the compositionally similar rhomb porphyry lavas. Larvikites to granites of the Siljan-Skrim plutonic complex belong to a younger generation formed at 282-277 Ma (Pedersen et al., 1995) and coincide with the eruption of trachytic lavas, one of which has been dated at 282.2±0.4 Ma (Corfu and Dahlgren, unpubl. data).

The youngest voluminous magmatic activity of the Oslo Rift was responsible for the emplacement of large syenitic to granitic batholiths which dominate the northern parts of the Graben. One of the concluding acts of this activity was the intrusion of the Tryvann granite at 259±1 Ma (Corfu and Dahlgren, unpubl. data). Although ages as young as 240 Ma have been reported for late intrusive activity (Sundvoll and Larsen, 1990; Sundvoll et al., 1990; Torsvik et al., 1998) there is some uncertainty as to whether all of these dates could be partially reset due to the locally intense hydrothermal activity that affected the Rift.

5.2. Magma sources and processes

Previous geochemical research demonstrated that the alkali basalts at Skien have elevated $^{206}Pb/^{204}Pb$ isotopic ratios, most similar to those of HIMU basalts found in some oceanic islands like St. Helena and Tubai (Anthony et al., 1989). The Pb compositions determined in this study for the Brunlanes and Skien units confirm these early observations yielding very radiogenic initial $^{206}Pb/^{204}Pb$ values of up to 21.29. In fact, after accounting for the older age of the suite, they rank among the most extreme radiogenic initial ratios on record (Fig. 4). In detail, there is a distinction between the basalts and the ignimbrite, the latter showing a value that is close to the Skien basalts whole rock values reported by Anthony et al. (1989). The variations probably reflect differences in the composition of the source and possibly crustal contributions.

The Skien volcanic suite analyzed by Anthony et al. (1989) yielded negative ε_{Sr} values, with ε_{Nd} progressively increasing from +1 and +4 from nephelinite to basanite and alkali basalt. The increasing ε_{Nd} correlates with decreasing abundances of Th, Nb, U, Ta and LREE. The mildly silica-saturated basalts of the Vestfold and Jeløya area (Fig. 1A) are characterized by ε_{Nd} values ranging mostly between +6 to +1 (Neumann et al., 2002) with very variable Sr isotopic compositions, which

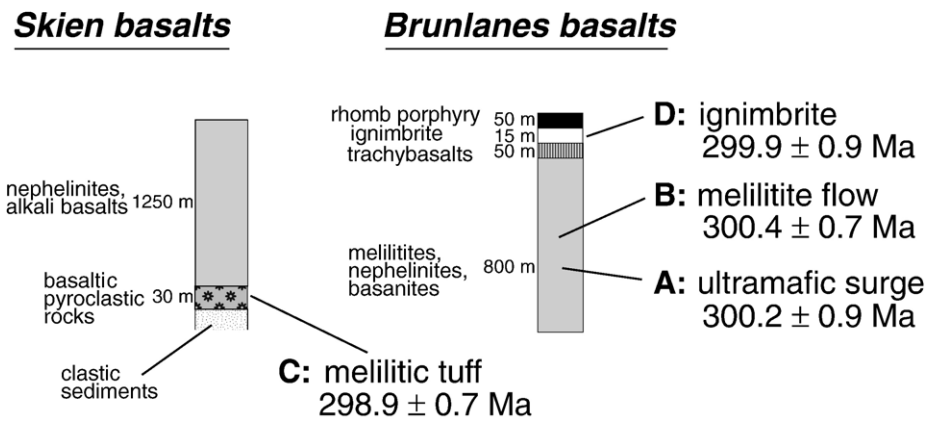

Fig. 5. Schematic profiles summarizing the ages and relationships of the dated units within the general stratigraphic succession.

probably reflect the effects of diagenesis and low-temperature alteration (Dunworth et al., 2001).

Neumann et al. (2004) proposed that the alkali basalts from Skien originated by small degrees of partial melting of mantle lithosphere, attributing their HIMU-type geochemical features to 'metasomatic enrichment by migrating carbonatitic fluids' related to the earlier formation of the nearby Fen complex at 580 Ma (Dahlgren, 1994). Although such a process can explain the very radiogenic Pb compositions, it is not evident whether it can also account for the very unradiogenic initial Sr compositions characteristic for this suite as the basalts are not especially depleted in Rb. Wilson et al. (1995) suggest that Central European melilitites could be formed in the Thermal Boundary Layer by low degrees of partial melting of carbonated phlogopite–garnet lherzolite at over 20 kbar and 1000–1200 °C. Their model involves enrichment of the Thermal Boundary Layer by partial melts from a HIMU mantle source prior to the formation of the melilitites in a process that leaves phlogopite (and amphibole) as stable residual phases, hence explaining an apparent deficit in K (Hegner et al., 1995; Dunworth and Wilson, 1998). Panter et al. (2006) discussed the origin of HIMU-type volcanic rocks in the South Pacific using a more complex multistage lithospheric model. An alternative is the traditional explanation of HIMU lavas as originating from recycled oceanic crust (Stracke et al., 2005).

The genesis of the Oslo Rift is most commonly discussed in terms of lithospheric extension and related mantle upwelling, decompression and partial melting (Pedersen and van der Beek, 1994; Neumann et al., 2004; Pascal et al., 2004). It has also been noted that the location of the rift was likely controlled by pre-existing structures of the Sveconorwegian orogen (Heeremans et al., 1996; Ebbing et al., 2005, 2007). The Rift coincides with a major down-step and eastward thickening of the lithosphere, and modeling shows that such an heterogeneity likely controlled the location of the rift during extension, necking the lithosphere and focusing the upwelling of the asthenosphere beneath the rift (Pascal et al., 2002, 2004). The model predicts that decompression will speed up as the stretching progresses with the potential to initiate rapid melting and generation of extensive basaltic melts, which is what is observed in the Rift at 300 Ma. There is a general resemblance between the sub-crustal structure of the Oslo Rift and that below the Baikal Rift. In the model discussed by Lebedev et al. (2006), however, there is the added factor that the astenosphere is convecting across the strike of the rift and, as it follows the step-up in the lithosphere, it rises and decompresses generating the basaltic magmas.

In the larger scale context the initial activity of the Olso Rift is one expression of contemporaneous, very widespread magmatism, basin formation and sedimentation in the foreland of the Variscan orogen and of late-tectonic magmatism at the interior of the orogen itself (e.g. Schaltegger and Corfu, 1995; Timmerman, 2004). These events accompanied the concluding stages of continental assembly that resulted in the supercontinent Pangea. The opening of many Permo-Carboniferous rifts, their arrangement in a radial manner converging towards the bending apex of the closing continental aggregation is considered to be an interrelated phenomenon reflecting the strain imposed on the lithosphere during convergence and plate self-subduction (Gutiérrez-Alonso et al., 2006).

6. Conclusions

U–Pb dating of perovskite (and titanite) has established precise and highly reproducible ages for the

otherwise geochronologically nearly intractable melilitic and nephelinitic volcanic rocks that represented the initiation of magmatism in the Oslo Rift. Data for the Brunlanes succession yield ages of 300.2±0.9, 300.4±0.7 and 299.9±0.9 Ma and a tuff at the base of Skien succession yields a slightly younger age of 298.9±0.7 Ma. These rocks are some 10 m.y. younger than underlying clastic sedimentary rocks belonging to the lower part of the Asker Group, but they were essentially coeval with its upper deltaic deposits (Gzhelian based on fossils). The common Pb compositions in the studied volcanic rocks are characterized by extremely high $^{206}Pb/^{204}Pb$ ratios that confirm the HIMU affinity of the source of these lavas.

Acknowledgments

Morten Schjoldager is thanked for preparing the mineral separates and Gunborg Bye Fjeld for assistance with the isotopic work. Martin Timmerman, editor Richard W. Carlson and an anonymous reviewer provided helpful comments and suggestions.

References

Anderson, D.L., 1994. The sublithospheric mantle as the source of continental flood basalts; the case against continental lithosphere and plume head reservoirs. Earth Planet. Sci. Lett. 123, 269–280.

Anthony, E.Y., Segalstad, T.V., Neumann, E.-R., 1989. An unusual mantle source region for nephelinites from the Oslo Rift, Norway. Geochim. Cosmochim. Acta 53, 1067–1076.

Bingen, B., Skår, Ø., Marker, M., Sigmond, E.M.O., Nordgulen, Ø., Ragnhildstveit, J., Mansfeld, J., Tucker, R.D., Liégeois, J.-P., 2005. Timing of continental building in the Sveconorwegian orogen, SW Scandinavia. Nor. J. Geol. 85, 87–116.

Corfu, F., Andersen, T.B., 2002. U–Pb ages of the Dalsfjord Complex, SW-Norway, and their bearing on the correlation of allochthonous crystalline segments of the Scandinavian Caledonides. Int. J. Earth Sci. 91, 955–963.

Dahlgren, S., 1994. Late Proterozoic and Carboniferous ultramafic magmatism of carbonatitic affinity in southern Norway. Lithos 31, 141–154.

Dahlgren, S., Corfu, F., 2001. Northward sediment transport from the late Carboniferous Variscan Mountains: zircon evidence from the Oslo Rift, Norway. J. Geol. Soc. 158, 29–36.

Dahlgren, S., Corfu, F., Heaman, L.M., 1996. U–Pb time constraints, and Hf and Pb source characteristics of the Larvik plutonic complex, Oslo Paleorift. Geodynamic and geochemical implications for the rift evolution. V.M. Goldschmidt Conf. J. Conf. Abstracts, vol. 120. Cambridge Publ.

Dunworth, E.A., Wilson, M., 1998. Olivine melilitites of the SW German Tertiary Volcanic Province: mineralogy and petrogenesis. J. Petrol. 39, 1805–1836.

Dunworth, E.A., Neumann, E.-R., Rosenbaum, J.M., 2001. The Skien lavas, Oslo Rift: petrological disequilibrium and geochemical evolution. Contrib. Mineral. Petrol. 140, 701–719.

Eagar, R.M.C., 1994. Non-marine bivalve assemblage in the Asker Group, Oslo Graben and its correlation with a late Pennsylvanian assemblage from North America. J. Geol. Soc. Lond. 151, 669–680.

Ebbing, J., Afework, Y., Olesen, O., Nordgulen, Ø., 2005. Is there evidence for magmatic underplating beneath the Oslo Rift? Terra Nova 17, 129–134.

Ebbing, J., Skilbrei, J.R., Olesen, O., 2007. Insights into the magmatic architecture of the Oslo Graben by petrophysically constrained analysis of the gravity and magnetic field. J. Geophys. Res. 112, B04404. doi:10.1029/2006JB004694.

Furman, T., Bryce, J.G., Karson, J., Iotti, A., 2004. East African Rift System (EARS) plume structure: insights from Quaternary mafic lavas of Turkana, Kenya. J. Petrol. 45, 1069–1088.

Gutiérrez-Alonso, G., Fernandez-Suarez, J., Weil, A.B., Murphy, J.B., Nance, R.D., Corfu, F., Johnston, S.T., 2006. Self-subduction of a global plate — the beginning of Pangea's end? Geol. Soc. Am., Ann. Meet., Abstr. 38/7, 237.

Gradstein, F.M., Ogg, J.G., Smith, A.G., et al., 2004. A Geologic Time Scale 2004. Cambridge University Press.

Heaman, L.M., 1989. The nature of the subcontinental mantle from Sr–Nd–Pb isotope studies on kimberlite perovskite. Earth Planet. Sci. Lett. 92, 323–334.

Heaman, L.M., Kjarsgaard, B.A., Creaser, R.A., 2004. The temporal evolution of North American kimberlites. Lithos 76, 377–397.

Heeremans, M., Larsen, B.T., Stel, H., 1996. Paleostress reconstruction from kinematic indicators in the Oslo Graben, southern Norway. New constraints on the mode of rifting. Tectonophysics 266, 55–79.

Hegner, E., Walter, H.J., Satir, M., 1995. Pb–Sr–Nd isotopic compositions and trace element geochemistry of megacrysts and melilitites from the Tertiary Urach volcanic field: source composition of small volume melts under SW Germany. Contrib. Mineral. Petrol. 122, 322–335.

Jaffey, A.H., Flynn, K.F., Glendenin, L.E., Bentley, W.C., Essling, A.M., 1971. Precision measurement of half-lives and specific activities of ^{235}U and ^{238}U. Phys. Rev., Sec. C, Nucl. Phys. 4, 1889–1906.

Kamo, S.L., Czamanske, G.K., Amelin, Y., Fedorenko, V.A., Davis, D.W., Trofimov, V.R., 2003. Rapid eruption of Siberian flood-volcanic rocks and evidence for coincidence with the Permian–Triassic boundary and mass extinction at 251 Ma. Earth Planet. Sci. Lett. 214, 75–91.

Lebedev, S., Meier, T., van der Hilst, R.D., 2006. Asthenospheric flow and origin of volcanism in the Baikal Rift area. Earth Planet. Sci. Lett. 249, 415–424.

Ludwig, K.R., 2003. Isoplot 3.0. A geochronological toolkit for Microsoft Excel: Berkeley Geochron. Center Spec. Publ., vol. 4. 70 p.

Neumann, E.-R., Tilton, G.R., Tuen, E., 1988. Sr, Nd and Pb isotope geochemistry of the Oslo rift igneous province, southeast Norway. Geochim. Cosmochim. Acta 52, 1997–2007.

Neumann, E.-R., Dunworth, E.A., Sundvoll, B.A., Tollefsrud, J.I., 2002. B1 basaltic lavas in Vestfold–Jeløya area, central Oslo rift: derivation from initial melts formed by progressive partial melting of an enriched mantle source. Lithos 61, 21–53.

Neumann, E.R., Wilson, M., Heeremans, M., Spencer, E.A., Obst, K., Timmerman, M.J., Kirstein, L., 2004. Carboniferous–Permian rifting and magmatism in southern Scandinavia, the North Sea and northern Germany: a review. In: Wilson, M., Neumann, E.R., Davies, G.R., Timmerman, M.J., Heeremans, M., Larsen, B.T. (Eds.), Permo-Carboniferous Magmatism and Rifting in Europe. Geol. Soc. London Spec. Publ., vol. 223, pp. 11–40.

Olaussen, S., Larsen, B.T., Steel, R., 1994. The Upper Carboniferous-Permian Oslo Rift; basin fill in relation to tectonic development. Can. Soc. Petrol. Geol. Mem. 17, 175–197.

Pallesen, S., 1994. Crustal extension in the Oslo Graben, SE Norway: a method incorporating magmatism and erosion. Tectonophysics 221, 155–117.

Panter, K.S., Blusztajn, J., Hart, S.R., Kyle, K.R., Esser, R., McIntosh, W.C., 2006. The origin of HIMU in the SW Pacific: evidence from intraplate volcanism in southern New Zealand and subantarctic islands. J. Petrol. 27, 1673–1704.

Pascal, C., van Wijk, J.W., Cloetingh, S.A.P.L., Davies, G.R., 2002. Effect of lithosphere thickness heterogeneities in controlling rift localization: numerical modeling of the Oslo Graben. Geophys. Res. Lett. 29, 1355. doi:10.1029/2001GL014354.

Pascal, C., Cloetingh, S.A.P.L., Davies, G.R., 2004. Asymmetric lithosphere as the cause of rifting and magmatism in the Permo-Carboniferous Oslo Graben. In: Wilson, M., Neumann, E.R., Davies, G.R., Timmerman, M.J., Heeremans, M., Larsen, B.T. (Eds.), Permo-Carboniferous Magmatism and Rifting in Europe. Geol. Soc. London Spec. Publ., vol. 223, pp. 139–156.

Pedersen, T., van der Beek, P., 1994. Extension and magmatism in the Oslo rift, southeast Norway: no sign of a mantle plume. Earth Planet. Sci. Lett. 123, 317–329.

Pedersen, L.E., Heaman, L.M., Holm, P.M., 1995. Further constraints on the temporal evolution of the Oslo rift from precise U–Pb zircon dating in the Siljan-Skrim area. Lithos 34, 301–315.

Petersen, J.S., 1978. Structure of the Larvikite–Lardalite Complex, Oslo-Region, Norway and its evolution. Geol. Rundsch. 67, 330–342.

Schaltegger, U., Corfu, F., 1995. Late Variscan "Basin and Range" magmatism and tectonics in the Central Alps: evidence form U–Pb geochronology. Geodin. Acta 8, 82–98.

Segalstad, T.V., 1979. Petrology of the Skien basaltic rocks, southwestern Oslo Region, Norway. Lithos 12, 221–239.

Späth, A., Le Roex, A.P., Opiyo-Akech, N., 2001. Plume-lithosphere interaction and the origin of continental rift-related alkaline volcanism — the Chyulu Hills Volcanic Province, Southern Kenya. J. Petrol. 42, 765–787.

Stracke, A., Hofmann, A.W., Hart, S.R., 2005. FOZO, HIMU, and the rest of the mantle zoo. Geochem. Geophys. Geosyst. 6, Q05007. doi:10.1029/2004gc000824.

Sundvoll, B., Larsen, B.T., 1990. Rb–Sr isotope systematics in the magmatic rocks of the Oslo Rift. Nor. Geol. Unders. Bull. 418, 27–46.

Sundvoll, B., Larsen, B.T., 1993. Rb–Sr and Sm–Nd relationships in dyke and sill intrusions in the Oslo Rift and related areas. Nor. Geol. Unders. Bull. 425, 25–41.

Sundvoll, B., Neumann, E.-R., Larsen, B.T., Tuen, E., 1990. Age relations among Oslo Rift magmatic rocks: implications for tectonic and magmatic modelling. Tectonophysics 178, 67–87.

Sundvoll, B., Larsen, B.T., Wandaas, B., 1992. Early magmatic phase in the Oslo Rift and its related stress regime. Tectonophysics 208, 37–54.

Timmerman, M.J., 2004. Timing, geodynamic setting and character of Permo-Carboniferous magmatism in the foreland of the Variscan Orogen, NW Europe. In: Wilson, M., Neumann, E.R., Davies, G.R., Timmerman, M.J., Heeremans, M., Larsen, B.T. (Eds.), Permo-Carboniferous Magmatism and Rifting in Europe. Geol. Soc. London Spec. Publ., vol. 223, pp. 41–74.

Torsvik, T.H., Eide, E.A., Meert, J.G., Smethurst, M.A., Walderhaug, H.J., 1998. The Oslo Rift: New palaeomagnetic and 40Ar/39Ar age constraints. J. Geophys. Int. 135, 1045–1059.

Torsvik, T.H., Smethurst, M.A., Burke, K., Steinberger, B., 2007. Long term stability in Deep Mantle structure: evidence from the ~300 Ma Skagerrak-Centered Large Igneous Province (the SCLIP). Geophys. Res. Abstr. 9 (EGU2007-A-04388).

Trønnes, R.G., Brandon, A.D., 1992. Mildly peraluminous high-silica granites in a continental rift: the Drammen and Finnemarka batholiths, Oslo Rift, Norway. Contrib. Mineral. Petrol. 109, 275–294.

White, R.S., McKenzie, D., 1989. Magmatism at rift zones: the generation of volcanic continental margins and flood basalts. J. Geophys. Res. B94, 7685–7729.

Wilson, M., Rosenbaum, J.M., Dunworth, E.A., 1995. Melilitites: partial melts of the thermal boundary layer? Contrib. Mineral. Petrol. 119, 181–196.